

Nonlinear point-coupling interaction for the relativistic Hartree-Bogoliubov approach

Zi Xin Liu^{a,b,c,*}, Yi Hua Lam^{a,b,*} and Ning Lu^{a,b,d}

^a*Institute of Modern Physics, Chinese Academy of Sciences, Lanzhou 730000, People's Republic of China*

^b*School of Nuclear Science and Technology, University of Chinese Academy of Sciences, Beijing 100049, People's Republic of China*

^c*School of Physics Science and Technology, Lanzhou University, Lanzhou 730000, People's Republic of China*

^d*School of Nuclear Science and Technology, Lanzhou University, Lanzhou 730000, People's Republic of China*

ARTICLE INFO

Keywords:

Nuclear Density Functional Theory
Relativistic Hartree-Bogoliubov
Point-coupling interactions
Binding energies and masses
Charge distribution
Saturation properties of nuclear matter
Neutron-rich nuclei

ABSTRACT

We propose a new nonlinear point-coupling parameterized interaction, PC-L3, for the relativistic Hartree-Bogoliubov framework with a separable pairing force by fitting to observables of 65 selected spherical nuclei, including the binding energies and charge radii. Overall, from comparing with the experimental data, the implementation of PC-L3 in relativistic Hartree-Bogoliubov successfully yields the lowest root-mean-square deviation, 1.251 MeV, among currently and commonly used point-coupling interactions. Meanwhile, PC-L3 is capable of estimating the saturation properties of the symmetric nuclear matter and of appropriately predicting the isospin and mass dependence of binding energy, e.g., the isotopes of $Z = 20, 50,$ and $82,$ and isotones of $N = 20, 50,$ and $82.$ The comparison of the estimated binding energies for ~ 5500 neutron-rich nuclei based on the PC-L3 and other point-coupling interactions is also presented.

1. Introduction

With the recent advancements in radioactive ion beams and detectors, new experiments have revealed a wealth of structural phenomena in exotic nuclei with extreme isospin values, such as the halo phenomena [1], island of inversion [2], neutron skin [3], the disappearance of traditional magic numbers but with the occurrence of new ones [4, 5], masses and half lives of the neutron-rich nuclei important for understanding the synthesis of heavy elements in extreme astrophysical environments [6], and masses of proton-rich nuclei for Type-I X-ray bursts [7]. Hence, theoretical nuclear models capable of providing a satisfactory description of the ground-state properties and collective excitations of atomic nuclei, ranging from the relatively light to superheavy nuclei, from the spherical to deformed nuclei, and from the valley of β -stability to the particle-drip lines [8, 9, 10, 11, 12, 13], are crucial for us to understand the interactions and configurations of nucleons in atomic nuclei.

The self-consistent relativistic mean-field (RMF) model with the Bardeen-Cooper-Schrieffer (BCS) method incorporating a nuclear density functional has been successfully used to describe various nuclear properties [14] and to obtain the relevant nuclear physics input for astrophysical calculations [15, 16, 17]. Such calculations were based on the RMF+BCS framework with the monopole pairing force, e.g., the δ pairing force [14, 18, 19, 20]. The BCS treatment on pairing force provides, however, a poor approximation for exotic nuclei far from the valley of β -stability [10]. The common understanding is that a consistent description of neutron-rich nuclei requires a unified and self-consistent treatment of mean-

field and pairing correlations, which plays a critical role in exotic nuclei. Therefore, the self-consistent relativistic Hartree-Bogoliubov (RHB) framework was developed to unify the treatment of pairing correlations and mean-field potentials, and to successfully analyze the structural phenomena in exotic nuclei [8, 21, 22, 23].

The most widely used effective interactions serving as the mean-field potential of the RMF and RHB frameworks are the meson-exchange [24, 25, 26, 27, 28, 29, 30]. In recent years, the point-coupling model offers an alternative to the meson-exchange model as the exchange of heavy mesons associated with short-distance dynamics cannot be resolved at low energies [14, 18, 31, 32, 33, 34, 35, 36, 37, 38, 39, 40]. The presently and commonly used point-coupling parameterized interactions include PC-PK1 [14], PC-F1 [18], PC-LA [31], and DD-PC1 [33]. The PC-LA parameterization does not consider a pairing force in the fitting procedure, whereas the PC-F1 and PC-PK1 interactions were fitted based on the RMF+BCS framework with the δ pairing force [14, 18, 19, 20]. The DD-PCX [35] and PC-X [36] interactions were recently proposed for the RHB model with a separable pairing force, however, its capability is yet to be assessed. Therefore, a point-coupling interaction accustomed to the RHB framework with the capability of describing the finite nuclei and nuclear matter properties close to experiment is highly desired by the community.

In this work, we propose a new set of nonlinear point-coupling interaction for the RHB framework with a separable pairing force, named PC-L3. We present the theoretical framework of the point-coupling interaction and relativistic Hartree-Bogoliubov model in Sec. 2. Then, we discuss the assessments of the new point-coupling interaction in Sec. 3, and further show the comparison of the nuclear binding energies resulted from various point-coupling interactions in Sec. 4. Our summary is drawn in Sec 5.

Corresponding authors:

liuzixin1908@impcas.ac.cn (Z.X. Liu); lanyihua@impcas.ac.cn (Y.H. Lam)

ORCID(s) 

0000-0001-5652-1516 (Z.X. Liu); 0000-0001-6646-0745 (Y.H. Lam);

0000-0002-3445-0451 (N. Lu)

2. Point-coupling interaction for the relativistic Hartree-Bogoliubov model

The effective covariant Lagrangian density of the point-coupling interaction for the relativistic mean field (RMF) model is expressed as [10, 11]

$$\mathcal{L} = \mathcal{L}^{\text{free}} + \mathcal{L}^{4f} + \mathcal{L}^{\text{ho}} + \mathcal{L}^{\delta} + \mathcal{L}^{\text{em}}, \quad (1)$$

where $\mathcal{L}^{\text{free}}$ is the free nucleons terms,

$$\mathcal{L}^{\text{free}} = \bar{\psi}(i\gamma_{\mu}\partial^{\mu} - M)\psi, \quad (2)$$

\mathcal{L}^{4f} is the four-fermion point-coupling terms,

$$\begin{aligned} \mathcal{L}^{4f} = & -\frac{1}{2}\alpha_S(\bar{\psi}\psi)(\bar{\psi}\psi) - \frac{1}{2}\alpha_V(\bar{\psi}\gamma_{\mu}\psi)(\bar{\psi}\gamma^{\mu}\psi) \\ & - \frac{1}{2}\alpha_{TV}(\bar{\psi}\vec{\tau}\gamma_{\mu}\psi) \cdot (\bar{\psi}\vec{\tau}\gamma^{\mu}\psi), \end{aligned} \quad (3)$$

\mathcal{L}^{ho} is the higher-order terms, which take into account of the effects of medium dependence,

$$\begin{aligned} \mathcal{L}^{\text{ho}} = & -\frac{1}{3}\beta_S(\bar{\psi}\psi)^3 - \frac{1}{4}\gamma_V[(\bar{\psi}\gamma_{\mu}\psi)(\bar{\psi}\gamma^{\mu}\psi)]^2 \\ & - \frac{1}{4}\gamma_S(\bar{\psi}\psi)^4, \end{aligned} \quad (4)$$

\mathcal{L}^{δ} is the gradient terms,

$$\begin{aligned} \mathcal{L}^{\delta} = & -\frac{1}{2}\delta_S\partial_{\nu}(\bar{\psi}\psi)\partial^{\nu}(\bar{\psi}\psi) - \frac{1}{2}\delta_V\partial_{\nu}(\bar{\psi}\gamma_{\mu}\psi)\partial^{\nu}(\bar{\psi}\gamma^{\mu}\psi) \\ & - \frac{1}{2}\delta_{TV}\partial_{\nu}(\bar{\psi}\vec{\tau}\gamma_{\mu}\psi)\partial^{\nu}(\bar{\psi}\vec{\tau}\gamma^{\mu}\psi), \end{aligned} \quad (5)$$

and \mathcal{L}^{em} is the electromagnetic interaction terms,

$$\mathcal{L}^{\text{em}} = -\frac{1}{4}F^{\mu\nu}F_{\mu\nu} - e\frac{(1-\tau_3)}{2}\bar{\psi}\gamma^{\mu}\psi A_{\mu}. \quad (6)$$

M in Eq. (2) is the nucleon mass. $\vec{\tau}$ in Eqs. (3) and (5) is the isospin vector of the third component, τ_3 . In Eqs. (3), (4), and (5), α_S , α_V , α_{TV} , β_S , γ_S , γ_V , δ_S , δ_V , and δ_{TV} are the respective coupling constants. The rotational symmetry of each coupling constant is indicated by the subscript. S and V refer to the scalar and vector nucleon fields, respectively. TV refers to the isovector fields. A_{μ} and $F_{\mu\nu}$ are the four-vector potential and field strength tensor of the electromagnetic field, respectively.

With implementing the effective Lagrangian density, the relativistic Hartree-Bogoliubov (RHB) model that unifies the self-consistent mean field and a pairing field had been developed to describe the properties of open-shell nuclei [8, 21, 22, 23]. Here, we use the point-coupling effective covariant Lagrangian density described above to be the self-consistent mean field of the RHB model, and take the separable form of the pairing force [35, 36, 41, 42] to be the pairing field. The RHB energy density functional is given as

$$E_{\text{RHB}}[\rho, \kappa] = E_{\text{RMF}}[\rho] + E_{\text{pair}}[\kappa], \quad (7)$$

where E_{RMF} is the self-consistent mean field term, and the pairing term reads

$$E_{\text{pair}}[\kappa] = \frac{1}{4} \sum_{n_1 n'_1} \sum_{n_2 n'_2} \kappa_{n_1 n'_1}^* \langle n_1 n'_1 | V^{pp} | n_2 n'_2 \rangle \kappa_{n_2 n'_2}, \quad (8)$$

where n refers to the original basis, e.g., an oscillator basis, or the coordinates in space, spin and isospin (\mathbf{r}, s, t) . The normal density, ρ , and the pairing tensor, κ are given as

$$\rho_{nn'} = \langle \Phi_0 | c_n^{\dagger} c_n | \Phi_0 \rangle, \text{ and } \kappa_{nn'} = \langle \Phi_0 | c_{n'} c_n | \Phi_0 \rangle, \quad (9)$$

respectively. $|\Phi_0\rangle$ is the ground state for an even-even nucleus. c_n^{\dagger} and c_n are the single-nucleon creation and annihilation operators, respectively. In the unitary Bogoliubov transformation, the single-nucleon operators is defined as the quasiparticle operators [43],

$$\beta_k^{\dagger} = \sum_n U_{nk} c_n^{\dagger} + V_{nk} c_n, \quad (10)$$

and $|\Phi_0\rangle$ is represented as a vacuum with respect to quasiparticles

$$|\Phi_0\rangle = \prod_k \beta_k |0\rangle, \quad (11)$$

and $|0\rangle$ is the bare vacuum.

The RHB equation for nucleons is derived by the variational procedure,

$$\int d^3\mathbf{r}' \begin{pmatrix} h_D - \lambda_{\tau} & \Delta \\ -\Delta^* & -h_D^* + \lambda_{\tau} \end{pmatrix} \begin{pmatrix} U_k \\ V_k \end{pmatrix} = E_k \begin{pmatrix} U_k \\ V_k \end{pmatrix}, \quad (12)$$

where E_k is the quasiparticle energy, λ_{τ} ($\tau = n, p$) is chemical potential, U_k and V_k are quasiparticle wave functions and h_D is the Dirac Hamiltonian,

$$h_D(\mathbf{r}) = \boldsymbol{\alpha} \cdot \mathbf{p} + V(\mathbf{r}) + \beta(M + S(\mathbf{r})), \quad (13)$$

and the scalar and vector potentials are

$$\begin{aligned} S(\mathbf{r}) &= \alpha_S \rho_S + \beta_S \rho_S^2 + \gamma_S \rho_S^3 + \delta_S \Delta \rho_S \text{ and} \\ V(\mathbf{r}) &= \alpha_V \rho_V + \gamma_V \rho_V^3 + \delta_V \Delta \rho_V + eA_0 \\ &\quad + \alpha_{TV} \tau_3 \rho_{TV} + \delta_{TV} \tau_3 \Delta \rho_{TV}, \end{aligned}$$

respectively. The local densities are

$$\begin{aligned} \rho_S(\mathbf{r}) &= \sum_{k>0} \bar{V}_k(\mathbf{r}) V_k(\mathbf{r}), \\ \rho_V(\mathbf{r}) &= \sum_{k>0} V_k^{\dagger}(\mathbf{r}) V_k(\mathbf{r}), \text{ and} \\ \rho_{TV}(\mathbf{r}) &= \sum_{k>0} V_k^{\dagger}(\mathbf{r}) \tau_3 V_k(\mathbf{r}). \end{aligned} \quad (14)$$

The pairing field Δ in Eq. (12) reads

$$\Delta_{n_1 n'_1} = \frac{1}{2} \sum_{n_2 n'_2} \langle n_1 n'_1 | V^{pp} | n_2 n'_2 \rangle \kappa_{n_2 n'_2}. \quad (15)$$

The pairing force that we use in Eq. (15) is the separable form of the pairing force, which is adjusted to model the pairing term of the finite range Gogny D1S force [44] in the particle-particle channel. The implementation of this separable form of the pairing force in the framework of RHB

Table 1

The PC-L3 point-coupling constants and pairing strengths.

Coupling constant	Quantity and physical unit(s)
α_S	$-3.96272 \times 10^{-04} \text{ MeV}^{-2}$
β_S	$8.6713 \times 10^{-11} \text{ MeV}^{-5}$
γ_S	$-3.81736 \times 10^{-17} \text{ MeV}^{-8}$
δ_S	$-1.17248 \times 10^{-10} \text{ MeV}^{-4}$
α_V	$2.6910 \times 10^{-04} \text{ MeV}^{-2}$
γ_V	$-3.74319 \times 10^{-18} \text{ MeV}^{-8}$
δ_V	$-4.26611 \times 10^{-10} \text{ MeV}^{-4}$
α_{TV}	$2.94218 \times 10^{-05} \text{ MeV}^{-2}$
δ_{TV}	$-4.08422 \times 10^{-10} \text{ MeV}^{-4}$
G	699.400 MeV fm^3
a	0.598 fm

model produces the pairing properties of the nuclear matter and of finite nuclei in the same footing as the effect yielded from the corresponding pairing Gogny interaction [41]. The separable form of the pairing force is expressed as

$$V^{pp}(\mathbf{r}_1, \mathbf{r}_2, \mathbf{r}'_1, \mathbf{r}'_2) = -G\delta(\mathbf{R} - \mathbf{R}')P(\mathbf{r})P(\mathbf{r}')\frac{1}{2}(1 - P^\sigma), \quad (16)$$

with the center of mass, $\mathbf{R} = (\mathbf{r}_1 + \mathbf{r}_2)/2$, and the relative coordinates, $\mathbf{r} = \mathbf{r}_1 - \mathbf{r}_2$. The form factor $P(\mathbf{r})$ is of Gaussian shape

$$P(\mathbf{r}) = \frac{1}{(4\pi a^2)^{3/2}} e^{-r^2/4a^2}. \quad (17)$$

According to Tian *et al.* [41], the G strength in Eq. (16) and the a parameter in Eq. (17) are defined as 728 MeV fm³ and 0.644 fm, respectively. We can in fact further optimize these G and a factors to improve the description of the bulk nuclear properties.

3. PC-L3, the optimized coupling constants and pairing strengths for the RHB model

We perform a series of calculations for 65 spherical nuclei to obtain a set of optimized coupling constants, and the G and a factors in the separable pairing force. The observables of 60 out of these 65 spherical nuclei were selected in the previous work to fit a point coupling interaction [14]. The configuration space of harmonic oscillator wave functions with appropriate symmetry is employed to solve the RHB equation for nucleons. The densities are computed in the coordinate space. The fermionic shells, $N_f = 20$, is adopted for these calculations. We name this new set of point-coupling interaction as PC-L3, which consists of the nine coupling constants in Eqs. (3), (4), and (5), and the G pairing strength and a factor in Eqs. (16) and (17). The new parameter set is listed in Table 1. We then assess the influence of the PC-L3 interaction on the ground state properties, i.e., binding energies and available charge radii of these 65 finite nuclei and the saturation properties of symmetric nuclear matter as follows.

Binding energies of the selected spherical nuclei – The experimental and theoretical binding energies of the selected 65 spherical nuclei are listed in Table 2. By comparing the rms deviation value in Table 2, we find that the present optimized PC-L3 interaction used in the RHB model with the separable pairing force yields the lowest rms deviation value, 1.251 MeV, among all theoretical models presented in Table 2. Using the PC-PK1, or PC-X, or DD-PC1, or DD-PCX, or PC-F1, or PC-LA interaction in the RHB model with the separable pairing force produces a rather high rms deviations, 1.421-3.050 MeV, comparing with the experimental binding energies (models labeled with a superscript asterisk in Table 2). Hereafter, the labels of all models with the specific point-coupling interaction and pairing force are referred to the footnote of Table 2, except when otherwise specified.

We remark that the RHB model with PC-PK1 interaction and separable pairing force produces an inverse order of the binding energies of ²¹⁴Ra and ²¹⁴Pb compared to experiment. By using the RHB model with PC-L3 interaction, the order is restored and comparable with experiment. The calculations of PC-PK1, PC-PK1[‡], and DD-PC1 listed in Table 2 also produce the same order as experiment but not the calculations of PC-PK1[‡], DD-PC1*, DD-PCX, PC-F1, PC-F1*, PC-LA, and PC-LA*.

Charge radii of the selected spherical nuclei – The theoretical radii of the selected spherical nuclei are compared with the updated experimental data, which was recently compiled by Angeli & Marinova [47] (see Table 4 in the Supplemental Material). Overall, the low rms deviations, 0.0194–0.025 fm, of comparing the calculated radii from each theoretical model with experimental radii indicate that all theoretical radii are in good agreement with experiment. The rms value of the RHB model with PC-L3 interaction, 0.0223 fm, even closely aligns with the rms values of other theoretical models (Table 4).

Saturation properties of the symmetric nuclear matter – We study the saturation properties and equation of state for the symmetric nuclear matter based on the covariant density functional of the PC-L3 interaction. These properties include the saturation density, ρ_0 , binding energy per nucleon, E/A , effective Dirac mass, M^* , incompressibility, K_0 , symmetry energy, E_{sym} , and slope of symmetry energy, L_0 .

Comparing the properties generated by PC-L3 with the ones resulted from other point-coupling interactions, i.e., PC-PK1 [14], PC-X [36], DD-PC1 [33], DD-PCX [35], PC-F1 [18], and PC-LA [31], overall, we find that all point-coupling interactions produce a set of rather similar ρ_0 with the average as $0.152^{+0.002}_{-0.004} \text{ fm}^{-3}$, and E/A with the average as $-16.11^{+0.06}_{-0.08} \text{ MeV}$ (Table 3). This indicates that PC-L3 not only exhibits the capability of describing the saturation properties of nuclear matter conformed with other nonlinear effective point-coupling interactions, but also agrees with the empirical $\rho_0 = 0.166 \pm 0.018 \text{ fm}^{-3}$ and $E/A = -16 \pm 1 \text{ MeV}$ [48]. Besides, we note that the nonlinear effective interactions PC-L3, PC-PK1, PC-F1, PC-LA, and PC-X produce a set of ρ_0 and E/A values somehow larger than the saturation properties produced by the density dependence

Table 2

The binding energies (in MeV) of the selected 65 spherical nuclei.

Nuclei	AME2020 ^a	PC-L3 ^b	PC-PK1 ^c	PC-PK1* ^d	PC-PK1 ^{±e}	PC-X ^f	DD-PC1 ^g	DD-PC1* ^h	DD-PCX ⁱ	PC-F1 ^j	PC-F1* ^k	PC-LA ^l	PC-LA* ^m
¹⁶ O	-127.619	-126.942	-127.280	-127.280	-127.29	-126.823	-128.527	-128.536	-127.297	-127.691	-127.691	-127.407	-127.654
¹⁸ Ne	-132.143	-132.794	-132.088	-132.664	-133.74	-132.278	-132.923	-133.423	-132.380	-132.216	-132.919	-132.317	-132.814
²⁰ Mg	-134.561	-135.584	-134.563	-135.347	-136.23	-134.961	-135.141	-135.780	-134.284	-134.613	-135.558	-134.992	-135.500
¹⁸ O	-139.513	-140.632	-140.223	-140.492	-141.63	-140.123	-141.145	-141.332	-140.523	-140.028	-140.693	-140.356	-140.636
²⁰ O	-151.371	-152.502	-151.962	-152.275	-153.16	-151.936	-152.790	-152.967	-151.802	-151.606	-152.390	-152.228	-152.488
²² O	-162.028	-162.641	-162.285	-162.583	-162.91	-162.191	-163.141	-163.288	-161.327	-162.054	-162.654	-162.665	-162.881
³⁶ Ca	-281.372	-281.350	-281.412	-281.495	-281.63	-280.409	-281.878	-281.977	-281.190	-282.001	-282.459	-280.454	-280.552
³⁴ Si	-283.464	-284.227	-284.727	-284.726	-284.63	-284.042	-285.967	-285.983	-284.752	-285.067	-285.025	-283.989	-284.261
³⁶ S	-308.714	-308.298	-308.374	-308.432	-308.55	-307.335	-309.305	-309.626	-308.996	-308.973	-309.389	-307.221	-307.721
³⁸ Ca	-313.122	-313.271	-313.230	-313.374	-313.46	-312.147	-314.501	-314.542	-313.554	-314.415	-314.934	-312.901	-312.984
³⁸ Ar	-327.343	-327.372	-327.107	-327.469	-327.54	-326.244	-328.691	-329.007	-328.003	-328.540	-329.020	-326.755	-327.207
⁴⁰ Ca	-342.052	-342.491	-343.060	-343.060	-343.07	-341.791	-345.113	-345.128	-343.258	-345.041	-345.041	-343.202	-343.428
⁴² Ti	-346.888	-348.330	-348.024	-348.343	-349.24	-347.219	-349.848	-350.069	-348.430	-349.701	-350.124	-348.626	-348.979
⁴² Ca	-361.896	-363.092	-363.142	-363.095	-364.06	-361.994	-365.143	-364.993	-363.688	-364.411	-364.179	-363.685	-363.712
⁴⁴ Ca	-380.960	-381.959	-381.915	-381.803	-382.77	-380.862	-383.967	-383.707	-382.480	-382.748	-383.215	-382.789	-382.764
⁴⁶ Ca	-398.773	-399.302	-399.451	-399.926	-399.86	-398.525	-401.668	-401.383	-399.914	-400.060	-400.367	-400.627	-400.670
⁴⁸ Ca	-416.001	-414.816	-415.492	-415.491	-415.39	-414.940	-417.973	-417.992	-415.990	-416.085	-416.030	-416.969	-417.382
⁵⁰ Ca	-427.508	-427.025	-426.937	-427.181	-427.34	-426.337	-428.660	-428.784	-427.022	-427.302	-427.797	-426.883	-427.194
⁵⁰ Ti	-437.786	-436.483	-436.445	-436.524	-437.27	-436.335	-437.761	-437.887	-436.996	-436.171	-436.417	-437.223	-437.763
⁵⁶ Ni	-483.996	-483.206	-483.669	-483.669	-483.68	-484.666	-481.447	-481.468	-481.821	-480.758	-480.758	-481.826	-482.479
⁵⁸ Ni	-506.460	-503.651	-503.636	-503.634	-504.08	-504.004	-502.587	-502.388	-503.241	-501.646	-502.055	-502.623	-502.870
⁷² Ni	-613.455	-614.920	-614.875	-614.662	-615.29	-613.790	-617.071	-616.648	-614.837	-614.646	-615.123	-614.486	-614.180
⁸⁴ Se	-727.339	-725.769	-725.732	-725.884	-726.28	-725.155	-728.792	-728.951	-726.274	-726.609	-726.976	-727.605	-727.924
⁸⁶ Kr	-749.235	-747.997	-747.939	-748.172	-748.46	-747.320	-751.050	-751.264	-748.759	-749.427	-749.832	-750.313	-750.709
⁸⁸ Sr	-768.468	-767.151	-767.138	-767.377	-767.64	-766.418	-770.240	-770.436	-768.244	-769.143	-769.496	-769.742	-770.140
⁹⁰ Zr	-783.897	-783.189	-783.033	-783.281	-783.72	-782.285	-785.806	-785.987	-784.319	-785.348	-785.635	-785.565	-785.952
⁹² Mo	-796.511	-796.452	-796.148	-796.368	-796.92	-795.510	-798.308	-798.467	-797.323	-798.191	-798.555	-798.719	-799.073
⁹⁴ Ru	-806.864	-807.307	-807.034	-807.190	-807.67	-806.537	-808.575	-808.683	-807.885	-808.731	-809.077	-809.695	-810.021
⁹⁸ Cd	-821.073	-822.442	-822.765	-822.799	-823.02	-822.633	-823.162	-823.200	-822.670	-823.668	-823.828	-825.580	-825.922
¹⁰⁰ Sn	-825.160	-826.806	-827.715	-827.716	-827.99	-827.832	-827.609	-827.638	-827.082	-828.156	-828.156	-830.582	-830.955
¹⁰⁶ Sn	-893.796	-891.844	-892.323	-891.392	-891.94	-890.686	-893.469	-892.254	-891.786	-893.370	-893.738	-895.447	-894.477
¹⁰⁸ Sn	-914.655	-912.334	-913.179	-911.731	-912.09	-910.846	-914.627	-912.926	-912.254	-914.236	-914.429	-916.165	-914.637
¹¹² Sn	-953.525	-951.378	-951.831	-950.787	-950.80	-949.647	-953.922	-952.645	-951.442	-953.367	-953.833	-954.258	-953.067
¹¹⁶ Sn	-988.682	-987.473	-987.601	-986.937	-986.84	-985.599	-990.019	-989.050	-987.673	-989.326	-989.950	-989.016	-987.950
¹²⁰ Sn	-1020.539	-1020.455	-1020.415	-1019.836	-1019.73	-1018.450	-1022.902	-1021.843	-1020.558	-1021.704	-1022.368	-1020.767	-1019.629
¹²² Sn	-1035.523	-1035.873	-1035.860	-1035.275	-1035.18	-1033.962	-1038.417	-1037.325	-1035.958	-1036.755	-1037.381	-1035.794	-1034.682
¹²⁴ Sn	-1049.958	-1050.625	-1050.715	-1050.128	-1050.02	-1048.938	-1053.402	-1052.321	-1050.782	-1051.160	-1051.717	-1050.327	-1049.289
¹²⁶ Sn	-1063.884	-1064.728	-1064.993	-1064.434	-1064.31	-1063.403	-1067.877	-1066.880	-1065.090	-1064.978	-1065.437	-1064.381	-1063.474
¹²⁸ Sn	-1077.372	-1078.181	-1078.688	-1078.214	-1078.11	-1077.372	-1081.835	-1081.030	-1078.925	-1078.234	-1078.567	-1077.945	-1077.246
¹³⁰ Sn	-1090.286	-1090.958	-1091.774	-1091.473	-1091.48	-1090.846	-1095.253	-1094.785	-1092.308	-1090.930	-1091.115	-1090.993	-1090.600
¹³² Sn	-1102.843	-1102.981	-1104.202	-1104.198	-1104.48	-1103.812	-1108.096	-1108.145	-1105.244	-1103.057	-1103.058	-1103.484	-1103.519
¹³⁴ Sn	-1108.873	-1109.018	-1109.253	-1109.583	-1109.62	-1109.141	-1112.253	-1112.306	-1109.487	-1107.330	-1107.965	-1106.707	-1106.791
¹³⁴ Te	-1123.408	-1123.845	-1124.205	-1124.543	-1124.96	-1123.898	-1128.176	-1128.474	-1125.408	-1124.193	-1124.631	-1124.613	-1124.869
¹³⁶ Xe	-1141.882	-1142.556	-1142.621	-1143.025	-1143.43	-1142.184	-1146.587	-1146.919	-1143.623	-1143.601	-1144.152	-1143.997	-1144.291
¹³⁸ Ba	-1158.292	-1159.185	-1159.381	-1159.628	-1159.99	-1158.637	-1163.283	-1163.477	-1159.896	-1161.245	-1161.646	-1161.575	-1161.777
¹⁴⁰ Ca	-1172.683	-1173.658	-1174.054	-1174.130	-1174.51	-1173.022	-1177.868	-1177.928	-1174.139	-1176.722	-1176.909	-1176.953	-1177.085
¹⁴² Nd	-1185.136	-1185.922	-1185.938	-1186.154	-1186.60	-1184.925	-1189.537	-1189.686	-1186.244	-1189.138	-1189.549	-1189.292	-1189.453
¹⁴⁴ Sm	-1195.730	-1196.123	-1195.736	-1196.090	-1196.50	-1194.786	-1199.024	-1199.262	-1196.280	-1199.353	-1199.961	-1199.420	-1199.623
¹⁴⁶ Gd	-1204.428	-1204.419	-1203.712	-1204.166	-1204.50	-1202.833	-1206.614	-1206.914	-1204.374	-1207.635	-1208.394	-1207.687	-1207.921
¹⁴⁸ Dy	-1210.779	-1210.921	-1209.974	-1210.497	-1210.73	-1209.166	-1212.454	-1212.793	-1210.639	-1214.117	-1214.993	-1214.258	-1214.510
¹⁵⁰ Er	-1215.330	-1215.715	-1214.624	-1215.189	-1215.29	-1213.878	-1216.686	-1217.044	-1215.191	-1218.943	-1219.890	-1219.236	-1219.501
²⁰⁰ Pb	-1576.362	-1574.040	-1574.885	-1573.842	-1572.71	-1572.812	-1577.817	-1576.199	-1574.372	-1575.666	-1576.251	-1575.769	-1574.487
²⁰² Pb	-1592.195	-1590.167	-1591.172	-1590.371	-1589.49	-1589.453	-1594.139	-1592.902	-1590.884	-1591.675	-1592.179	-1591.240	-1590.260
²⁰⁴ Pb	-1607.506	-1605.842	-1607.068	-1606.540	-1606.05	-1605.740	-1610.026	-1609.231	-1606.984	-1607.325	-1607.708	-1606.187	-1605.541
²⁰⁶ Hg	-1621.049	-1620.450	-1621.321	-1621.724	-1621.79	-1621.173	-1623.820	-1624.168	-1621.236	-1620.353	-1620.916	-1616.956	-1617.093
²⁰⁶ Pb	-1622.325	-1621.002	-1622.525	-1622.282	-1622.32	-1621.600	-1625.385	-1625.065	-1622.583	-1622.563	-1622.779	-1620.490	-1624.189
²⁰⁸ Pb	-1636.430	-1635.516	-1637.438	-1637.432	-1637.92	-1636.842	-1640.008	-1640.059	-1637.456	-1637.241	-1637.240	-1633.865	-1633.788
²¹⁰ Pb	-1645.553	-1644.342	-1645.449	-1645.470	-1645.59	-1644.752	-1648.272	-1647.790	-1644.858	-1644.793	-1645.176	-1641.484	-1640.774
²¹⁰ Po	-1645.213	-1645.615	-1646.703	-1646.941	-1647.25	-1646.050	-1649.441	-1649.613	-1646.598	-1647.760	-1648.128	-1644.643	-1644.639
²¹² Pb	-1654.516	-1652.921	-1653.425	-1653.428	-1653.19	-1652.600	-1656.428	-1655.456	-1652.128	-1652.275	-1652.946	-1648.887	-1647.639
²¹² Rn	-1652.497	-1653.877	-1654.632	-1654.938	-1655.11	-1653.796	-1657.476	-1657.670	-1654.199	-1656.863	-1657.348	-1653.921	-1653.943
²¹⁴ Ra	-1658.323	-1660.465	-1661.172	-1661.459	-1661.55	-1660.102	-1664.092	-1664.266	-1660.290	-1664.512	-1664.978	-1661.709	-1661.740
²¹⁴ Pb	-1663.293	-1661.294	-1661.397	-1661.307	-1660.73	-1660.390	-1664.481	-1663.050	-1659.279	-1659.697	-1660.556	-1656.073	-1654.381
²¹⁶ Th	-1662.695	-1665.373	-1666.248	-1666.463	-1666.59	-1664.923	-1669.244	-1669.374	-1664.832	-1670.649	-1670.995	-1667.967	-1668.001
²¹⁸ U	-1665.677	-1668.505	-1669.602	-1669.695	-1670.05	-1668.007	-1672.733	-1672.770	-1667.664	-1675.109	-1675.138	-1672.491	-1672.522
rms ⁿ		1.251	1.312	1.471	1.69	1.587	3.088	3.050	1.421	2.584	2.782	2.609	2.838

^a The experimental binding energies compiled in AME2020 [45].

^b PC-L3: calculated from the RHB model with the PC-L3 interaction.

^c PC-PK1: quoted from the RMF model with the Bardeen-Cooper-S

Table 3

The saturation properties of nuclear matter estimated by the nonlinear point-coupling interactions, i.e., PC-L3, PC-PK1 [14], PC-X [36], PC-F1 [18], and PC-LA [31] and the density-dependent point-coupling interactions, DD-PC1 [33] and DD-PCX [35].

	PC-L3	PC-PK1	PC-X	DD-PC1	DD-PCX	PC-F1	PC-LA
ρ_0 (fm^{-3})	0.154	0.154	0.154	0.152	0.152	0.151	0.148
E/A (MeV)	-16.13	-16.12	-16.14	-16.06	-16.03	-16.17	-16.13
M^*/M	0.59	0.59	0.58	0.58	0.56	0.61	0.58
K_0 (MeV)	239	238	240	230	213	255	264
E_{sym} (MeV)	35.8	35.6	35.2	33	31	37.8	37.2
L_0 (MeV)	114	113	112	70	46	117	108

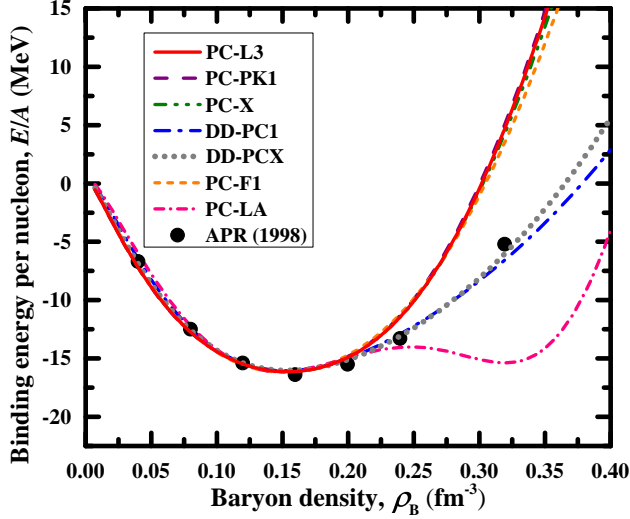


Figure 1: The binding energy per nucleon, E/A , for the nuclear matter as a function of the baryon density, ρ_B , see texts.

point-coupling interactions, DD-PC1 and DD-PCX.

Figure 1 displays the binding energy curves for symmetric nuclear matter produced from the PC-L3, PC-PK1, PC-X, DD-PC1, DD-PCX, PC-F1, and PC-LA interactions, and the *ab initio* variational calculations (black dots) [49]. For the baryon density $\rho_B \leq 0.20$, the E/A predicted by PC-L3 is consistent with all point-coupling interactions and the *ab initio* variational calculation owing to the constraints from the properties of finite nuclei. For the high density region with $\rho_B \geq 0.30$, the DD-PCX binding energy curve is closer to the prediction from the *ab initio* variational calculation, while softer than those from the PC-L3, PC-PK1, PC-X, and PC-F1 interactions, and stiffer than the one from the DD-PC1, and PC-LA interactions. Note that the inconsistent description at the high-density nuclear matter region, $\rho_B \geq 0.30$, is not sensitive on the description of the low-energy bulk nuclear properties.

4. Binding energies of spherical nuclei

Binding energies of isotopic and isotonic chains –

We present the comparison of the experimental and theoretical binding energies for some isotopic and isotonic chains based on the point-coupling interactions PC-L3, PC-PK1, PC-X, DD-PC1, and DD-PCX used in the RHB, RMF, and RCHB frameworks in Fig. 2. For the $Z=20$ (Ca) isotopes, $N=20$ and $N=50$ isotones, the results from PC-L3, PC-

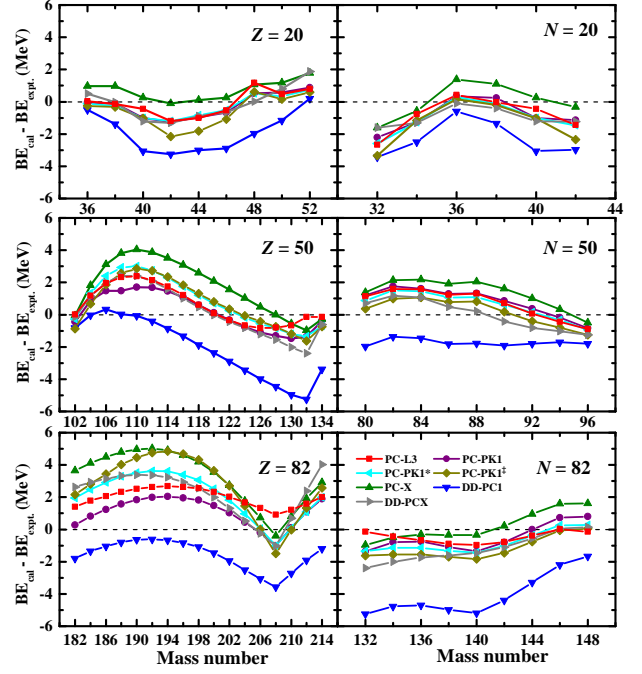


Figure 2: The deviations between the AME2020 experimental data [45] and the calculated binding energies for the $Z=20$, 50, and 82 isotopes, and for the $N=20$, 50, and 82 isotones. See the footnote of Table 2 for the theoretical frameworks labeled in this figure. The data of PC-PK1 (purple dots) and DD-PC1 (blue down triangles) are quoted from Ref. [14], whereas the PC-PK1 ‡ data is from Ref. [46].

PK1, and PC-PK1* are rather similar, whereas for the $Z=50$ (Sn) and $Z=82$ (Pb) isotopes, especially for the even-even $^{122-134}\text{Sn}$, the PC-PK1* produces a set of binding energies more deviated from experiment compared to PC-L3 and PC-PK1, indicating the superiority of PC-L3 accustomed to the RHB model that yields an overall agreement with the prediction of PC-PK1 used in the RMF+BCS framework. We remark that a steep change at ^{208}Pb is produced by PC-PK1, PC-PK1*, PC-PK ‡ , PC-X, DD-PC1, and DD-PCX, whereas PC-L3 results a more consistent deviation (lower left panel in Fig. 2). A similar characteristic also happens in the $Z=50$ isotopic chain at ^{132}Sn . For the $N=82$ isotones, PC-L3 reproduces the experimental binding energies with the average absolute deviation 0.494 MeV, whereas PC-PK1, PC-PK1*, PC-PK ‡ , PC-X, DD-PC1, and DD-PCX produce the average absolute deviation of 0.854 MeV, 1.18 MeV, 0.926 MeV, 0.757 MeV, 4.051 MeV, and 1.228 MeV, respectively. This implies that PC-L3 is able to balance the Coulomb field and the isovector channel of the effective Lagrangian. Thus, PC-L3 provides an appropriate prediction for not only the binding energy but also the isospin dependence.

Binding energies of spherical nuclei – We also compute and compare the binding energies of ~ 5500 neutron-rich nuclei using the RHB model with the PC-L3 (or PC-PK1) interaction with a separable pairing force (Fig. 3A). The comparison of both binding energies from PC-L3 and PC-PK1 ‡ is given in Fig. 3B. For the present calculations of odd- N and/or odd- Z nuclei, we consider the blocking ef-

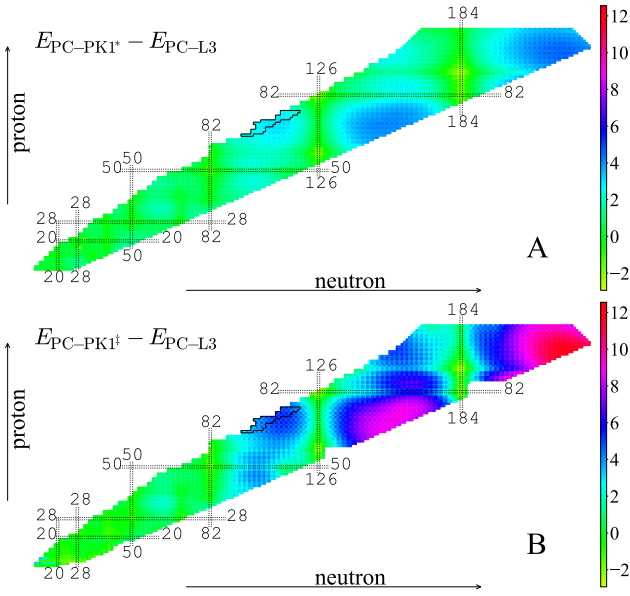


Figure 3: The deviations of the binding energies of neutron-rich nuclei produced by the PC-PK1* (A) or PC-PK1[‡] (B) with the binding energies calculated from the PC-L3. See the footnote of Table 2 for the theoretical frameworks of PC-PK1*, PC-PK1[‡], and PC-L3.

fects of the unpaired nucleon(s)¹. For the light to medium nuclei at the region $Z = 8-50$ and $N = 20-126$, the PC-L3 results are considerable close to the ones of PC-PK1* and PC-PK1[‡], except at the region $Z=28-50$ and $N=82-126$ for PC-PK1[‡]. We compare the theoretical energies with currently available experimental data [45] at the region $Z=65-75$ and $N = 95-120$, encircled with the black line in Figs. 3A and 3B. The root of relative square (rrs) deviation² for PC-L3, PC-PK1*, and PC-PK1[‡] is 0.954%, 1.142%, and 1.249%, respectively.

For the heavy nuclei far from stability at regions $Z=50-82$ and $N = 126-184$, PC-PK1* (PC-PK1[‡]) estimates a set of binding energies, up to 4.369 MeV (9.342 MeV) larger than the energies produced from PC-L3. Meanwhile, for the region at $Z>82$ and $N>184$, the binding energies produced from PC-PK1* and PC-PK1[‡] further deviate from the ones generated by PC-L3; for PC-PK1* and PC-PK1[‡], the largest absolute deviation is 4.801 MeV and 12.549 MeV, respectively. We anticipate that the RHB with the consideration of axial symmetry or triaxial deformation could further reduce the deviation between the theoretical and experiment binding energies for the region $Z=65-75$ and $N=95-120$.

5. Summary

In this work, we propose a new nonlinear point-coupling parameterized interaction, PC-L3, for the RHB framework

¹The ground state of a nucleus with an odd neutron and/or proton number is one-quasiparticle state, $|\Phi_1\rangle = \beta_{i_b}^\dagger |\Phi_0\rangle$, which is constructed based on the ground state of an even-even nucleus $|\Phi_0\rangle$, c.f. Eq. (11), where β^\dagger is the single-nucleon creation operator and i_b denotes the blocked quasiparticle state occupied by the unpaired nucleon(s). See Ref. [43] for the detail description of using the blocking effect. The same technique is employed for calculating the mirror displacement energies along the $N = Z$ line [7].

²root of relative square = $\sqrt{(\sum_i (E_i^{\text{expt.}} - E_i^{\text{calc.}})^2 / (E_i^{\text{expt.}})^2) / N}$.

with a separable pairing force (Table 1). The PC-L3 interaction is fitted to the observables of 65 selected spherical nuclei, i.e., the binding energies and charge radii. The lowest rms deviation, 1.251 MeV, yielded by the implementation of the PC-L3 interaction in the RHB framework with the separable pairing force indicates the capability and feasibility of PC-L3 in the RHB framework unifying the treatment of pairing correlations and mean-field potentials, compared to other point-coupling interactions, i.e., PC-PK1, PC-X, DD-PC1, DD-PCX, PC-F1, and PC-LA, which are either used in the RHB framework with the separable pairing force or the RMF+BCS framework with the δ pairing force, or PC-PK1 used in the RCHB framework with the δ pairing force (Table 2). Meanwhile, the PC-L3 for the RHB framework provides the same description as other point-coupling interactions for the charge radii of the selected 23 spherical nuclei, and produces a set of charge radii in a good agreement with experiment. A set of similar saturation properties is also obtained for the symmetric nuclear matter using the PC-L3 interaction, compared to the saturation properties generated from other point-coupling interactions.

We compare the experimental binding energies of the $Z = 20, 50$, and 82 isotopic and $N = 20, 50$, and 82 isotonic chains with the theoretical values resulted from the point-coupling interactions, PC-L3, PC-PK1, PC-X, DD-PC1, and DD-PCX used in RHB, RMF+BCS, and RCHB frameworks. The PC-L3 provides an appropriate prediction for not only the binding energy but also for the isospin dependence. Meanwhile, the binding energies of ~ 5500 neutron-rich nuclei computed from the RHB model with the PC-L3 interaction are compared with the results generated from the RCHB model with the PC-PK1 interaction [46]. The binding energies produced from PC-L3, PC-PK1*, and PC-PK1[‡] are rather close at the relatively light region. For the heavy region at $Z=65-75$ and $N=95-120$, the PC-L3 provides the lowest rrs deviation, 0.954%, among PC-L3, PC-PK1*, and PC-PK1[‡], comparing with the currently available 70 experimental nuclear masses. We anticipate that PC-L3 could be a competently alternative point-coupling interaction for the RHB framework.

Declaration of competing interest

The authors declare that they have no known competing financial interests or personal relationships that could have appeared to influence the work reported in this paper.

Acknowledgments

This work was financially supported by the Strategic Priority Research Program of Chinese Academy of Sciences (CAS, Grant Nos. XDB34000000) and National Natural Science Foundation of China (No. 11775277). We are appreciative of the computing resource provided by the Institute of Physics (PHYS_T3 cluster) and the Academia Sinica Grid-computing Center Distributed Cloud resources (QDR4 and FDR5 clusters) of Academia Sinica, Taiwan. Part of the numerical calculations were performed at the Gansu Advanced

Computing Center. YHL gratefully acknowledges the financial supports from the Chinese Academy of Sciences President's International Fellowship Initiative (No. 2019FYM0002) and appreciates the laptop (Dell M4800) partially sponsored by Pin-Kok Lam and Fong-Har Tang during the pandemic of COVID-19.

A. Supplementary material

Supplementary material related to this article is attached in this preprint.

CRedit authorship contribution statement

Zi Xin Liu: Conceptualization of this study, Fitting PC-RHB, Writing - Original draft preparation. **Yi Hua Lam:** Conceptualization of this study, Fitting PC-RHB, Writing - Original draft preparation. **Ning Lu:** Writing - Original draft preparation.

References

- [1] I. Tanihata, H. Savajols, R. Kanungo, *Prog. Part. Nucl. Phys.* 68 (2013) 215. URL: <https://www.sciencedirect.com/science/article/pii/S0146641012001081>. doi:10.1016/j.pnnp.2012.07.001.
- [2] F. Nowacki, A. Obertelli, A. Poves, *Prog. Part. Nucl. Phys.* 120 (2021) 103866. URL: <https://www.sciencedirect.com/science/article/pii/S014664102100020X>. doi:10.1016/j.pnnp.2021.103866.
- [3] H. Sakaguchi, J. Zenihiro, *Prog. Part. Nucl. Phys.* 97 (2017) 1. URL: <https://www.sciencedirect.com/science/article/pii/S0146641017300546>. doi:10.1016/j.pnnp.2017.06.001.
- [4] A. Ozawa, T. Kobayashi, T. Suzuki, K. Yoshida, I. Tanihata, *Phys. Rev. Lett.* 84 (2000) 5493. URL: <https://link.aps.org/doi/10.1103/PhysRevLett.84.5493>. doi:10.1103/PhysRevLett.84.5493.
- [5] F. Wienholtz, D. Beck, K. Blaum, Ch. Borgmann, M. Breitenfeldt, R. B. Cakirli, S. George, F. Herfurth, J. D. Holt, M. Kowalska, S. Kreim, D. Lunney, V. Manea, J. Menéndez, D. Neidherr, M. Rosenbusch, L. Schweikhard, A. Schwenk, J. Simonis, J. Stanja, R. N. Wolf, K. Zuber, *Nature* 498 (2013) 346. URL: <https://www.nature.com/articles/nature12226>. doi:10.1038/nature12226.
- [6] T. Marketin, L. Huther, G. Martínez-Pinedo, *Phys. Rev. C* 93 (2016) 025805. URL: <https://link.aps.org/doi/10.1103/PhysRevC.93.025805>. doi:10.1103/PhysRevC.93.025805.
- [7] Y. H. Lam, Z. X. Liu, A. Heger, N. Lu, A. M. Jacobs, Z. Johnston, to appear at *Astrophys. J.* arXiv: 2110.13676 (2022). URL: <https://arxiv.org/abs/2110.13676>.
- [8] P. Ring, *Prog. Part. Nucl. Phys.* 37 (1996) 193. URL: <https://www.sciencedirect.com/science/article/pii/0146641096000543>. doi:10.1016/0146-6410(96)00054-3.
- [9] M. Bender, P.-H. Heenen, P.-G. Reinhard, *Rev. Mod. Phys.* 75 (2003) 121. URL: <https://link.aps.org/doi/10.1103/RevModPhys.75.121>. doi:10.1103/RevModPhys.75.121.
- [10] D. Vretenar, A. V. Afanasjev, G. A. Lalazissis, P. Ring, *Phys. Rep.* 409 (2005) 101. URL: <https://www.sciencedirect.com/science/article/pii/S0370157304004545>. doi:10.1016/j.physrep.2004.10.001.
- [11] J. Meng, H. Toki, S.-G. Zhou, S. Q. Zhang, W. H. Long, L. S. Geng, *Prog. Part. Nucl. Phys.* 57 (2006) 470. URL: <https://www.sciencedirect.com/science/article/pii/S014664100500075X>. doi:10.1016/j.pnnp.2005.06.001.
- [12] T. Nikšić, D. Vretenar, P. Ring, *Prog. Part. Nucl. Phys.* 66 (2011) 519. URL: <https://www.sciencedirect.com/science/article/pii/S0146641011000561>. doi:10.1016/j.pnnp.2011.01.055.
- [13] J. Meng, S.-G. Zhou, J. Phys. G: Nucl. Part. Phys. 42 (2015) 093101. URL: <https://doi.org/10.1088/0954-3899/42/9/093101>. doi:10.1088/0954-3899/42/9/093101.
- [14] P. W. Zhao, Z. P. Li, J. M. Yao, J. Meng, *Phys. Rev. C* 82 (2010) 054319. URL: <https://link.aps.org/doi/10.1103/PhysRevC.82.054319>. doi:10.1103/PhysRevC.82.054319.
- [15] B. Sun, F. Montes, L. S. Geng, H. Geissel, Y. A. Litvinov, J. Meng, *Phys. Rev. C* 78 (2008) 025806. URL: <https://link.aps.org/doi/10.1103/PhysRevC.78.025806>. doi:10.1103/PhysRevC.78.025806.
- [16] Z. M. Niu, B. Sun, J. Meng, *Phys. Rev. C* 80 (2009) 065806. URL: <https://link.aps.org/doi/10.1103/PhysRevC.80.065806>. doi:10.1103/PhysRevC.80.065806.
- [17] X. D. Xu, B. Sun, Z. M. Niu, Z. Li, Y.-Z. Qian, J. Meng, *Phys. Rev. C* 87 (2013) 015805. URL: <https://link.aps.org/doi/10.1103/PhysRevC.87.015805>. doi:10.1103/PhysRevC.87.015805.
- [18] T. Bürvenich, D. G. Madland, J. A. Maruhn, P.-G. Reinhard, *Phys. Rev. C* 65 (2002) 044308. URL: <https://link.aps.org/doi/10.1103/PhysRevC.65.044308>. doi:10.1103/PhysRevC.65.044308.
- [19] T. Nikšić, D. Vretenar, P. Ring, *Phys. Rev. C* 73 (2006) 034308. URL: <https://link.aps.org/doi/10.1103/PhysRevC.73.034308>. doi:10.1103/PhysRevC.73.034308.
- [20] T. Nikšić, D. Vretenar, P. Ring, *Phys. Rev. C* 74 (2006) 064309. URL: <https://link.aps.org/doi/10.1103/PhysRevC.74.064309>. doi:10.1103/PhysRevC.74.064309.
- [21] H. Kucharek, P. Ring, *Z. Phys. A* 339 (1991) 23. URL: <https://link.springer.com/article/10.1007/BF01282930>. doi:10.1007/BF01282930.
- [22] J. Meng, P. Ring, *Phys. Rev. Lett.* 77 (1996) 3963. URL: <https://link.aps.org/doi/10.1103/PhysRevLett.77.3963>. doi:10.1103/PhysRevLett.77.3963.
- [23] W. Pöschl, D. Vretenar, G. A. Lalazissis, P. Ring, *Phys. Rev. Lett.* 79 (1997) 3841. URL: <https://link.aps.org/doi/10.1103/PhysRevLett.79.3841>. doi:10.1103/PhysRevLett.79.3841.
- [24] G. A. Lalazissis, J. König, P. Ring, *Phys. Rev. C* 55 (1997) 540. URL: <https://link.aps.org/doi/10.1103/PhysRevC.55.540>. doi:10.1103/PhysRevC.55.540.
- [25] S. Typel, H. H. Wolter, *Nucl. Phys. A* 656 (1999) 331. URL: <https://www.sciencedirect.com/science/article/pii/S0375947499003103>. doi:10.1016/S0375-9474(99)00310-3.
- [26] T. Nikšić, D. Vretenar, P. Finelli, P. Ring, *Phys. Rev. C* 66 (2002) 024306. URL: <https://link.aps.org/doi/10.1103/PhysRevC.66.024306>. doi:10.1103/PhysRevC.66.024306.
- [27] H. Abusara, A. V. Afanasjev, P. Ring, *Phys. Rev. C* 85 (2012) 024314. URL: <https://link.aps.org/doi/10.1103/PhysRevC.85.024314>. doi:10.1103/PhysRevC.85.024314.
- [28] M. Dutra, O. Lourenço, S. S. Avancini, B. V. Carlson, A. Delfino, D. P. Menezes, C. Providência, S. Typel, J. R. Stone, *Phys. Rev. C* 90 (2014) 055203. URL: <https://link.aps.org/doi/10.1103/PhysRevC.90.055203>. doi:10.1103/PhysRevC.90.055203.
- [29] W.-L. Lu, Z.-X. Liu, S.-H. Ren, W. Zhang, T.-T. Sun, *J. Phys. G: Nucl. Part. Phys.* 44 (2017) 125104. URL: <https://doi.org/10.1088/1361-6471/aa8e2d>. doi:10.1088/1361-6471/aa8e2d.
- [30] Z.-X. Liu, C.-J. Xia, W.-L. Lu, Y.-X. Li, J. N. Hu, T.-T. Sun, *Phys. Rev. C* 98 (2018) 024316. URL: <https://link.aps.org/doi/10.1103/PhysRevC.98.024316>. doi:10.1103/PhysRevC.98.024316.
- [31] B. A. Nikolaus, T. Hoch, D. G. Madland, *Phys. Rev. C* 46 (1992) 1757. URL: <https://link.aps.org/doi/10.1103/PhysRevC.46.1757>. doi:10.1103/PhysRevC.46.1757.
- [32] J. J. Ruskak, R. J. Furnstahl, *Nucl. Phys. A* 627 (1997) 495. URL: <https://www.sciencedirect.com/science/article/pii/S0375947497005988>. doi:10.1016/S0375-9474(97)00598-8.
- [33] T. Nikšić, D. Vretenar, P. Ring, *Phys. Rev. C* 78 (2008) 034318. URL: <https://link.aps.org/doi/10.1103/PhysRevC.78.034318>. doi:10.1103/PhysRevC.78.034318.
- [34] J. Zhao, B.-N. Lu, E.-G. Zhao, S.-G. Zhou, *Phys. Rev. C* 95 (2017) 014320. URL: <https://link.aps.org/doi/10.1103/PhysRevC.95.014320>. doi:10.1103/PhysRevC.95.014320.
- [35] E. Yüksel, T. Marketin, N. Paar, *Phys. Rev. C* 99 (2019) 034318. URL: <https://link.aps.org/doi/10.1103/PhysRevC.99.034318>. doi:10.1103/PhysRevC.99.034318.
- [36] A. Taninah, S. E. Agbemava, A. V. Afanasjev, P. Ring, *Phys. Lett. B* 800 (2020) 135065. URL: <https://www.sciencedirect.com/science/>

Supplementary material

- [article/pii/S0370269319307877](https://doi.org/10.1016/j.physletb.2019.135065). doi:10.1016/j.physletb.2019.135065.
- [37] U. C. Perera, A. V. Afanasjev, P. Ring, Phys. Rev. C 104 (2021) 064313. URL: <https://link.aps.org/doi/10.1103/PhysRevC.104.064313>. doi:10.1103/PhysRevC.104.064313.
- [38] D. Vale, Y. F. Niu, N. Paar, Phys. Rev. C 103 (2021) 064307. URL: <https://link.aps.org/doi/10.1103/PhysRevC.103.064307>. doi:10.1103/PhysRevC.103.064307.
- [39] F. Ji, J. Hu, H. Shen, Phys. Rev. C 103 (2021) 055802. URL: <https://link.aps.org/doi/10.1103/PhysRevC.103.055802>. doi:10.1103/PhysRevC.103.055802.
- [40] K. Zhang, M.-K. Cheoun, Y.-B. Choi, P. S. Chong, J. Dong, Z. Dong, X. Du, L. Geng, E. Ha, X.-T. He, C. Heo, M. C. Ho, E. J. In, S. Kim, Y. Kim, C.-H. Lee, J. Lee, H. Li, Z. Li, T. Luo, J. Meng, M.-H. Mun, Z. Niu, C. Pan, P. Papakonstantinou, X. Shang, C. Shen, G. Shen, W. Sun, X.-X. Sun, C. K. Tam, Thavayongnou, C. Wang, X. Wang, S. H. Wong, J. Wu, X. Wu, X. Xia, Y. Yan, R. W.-Y. Yeung, T. C. Yiu, S. Zhang, W. Zhang, X. Zhang, Q. Zhao, S.-G. Zhou, At. Data Nucl. Data Tables 144 (2022) 101488. URL: <https://www.sciencedirect.com/science/article/pii/S0092640X22000018>. doi:10.1016/j.adt.2022.101488.
- [41] Y. Tian, Z. Y. Ma, P. Ring, Phys. Lett. B 676 (2009) 44. URL: <https://www.sciencedirect.com/science/article/pii/S0370269309004912>. doi:10.1016/j.physletb.2009.04.067.
- [42] Y. Tian, Z.-y. Ma, P. Ring, Phys. Rev. C 79 (2009) 064301. URL: <https://link.aps.org/doi/10.1103/PhysRevC.79.064301>. doi:10.1103/PhysRevC.79.064301.
- [43] P. Ring, P. Schuck, The Nuclear Many-body Problem, Springer-Verlag, 1980.
- [44] J. F. Berger, M. Girod, D. Gogny, Nucl. Phys. A 428 (1984) 23. URL: <https://www.sciencedirect.com/science/article/pii/0375947484902409>. doi:10.1016/0375-9474(84)90240-9.
- [45] F. G. Kondev, M. Wang, W. J. Huang, S. Naimi, G. Audi, Chin. Phys. C 45 (2021) 030001. URL: <https://doi.org/10.1088/1674-1137/abddae>. doi:10.1088/1674-1137/abddae.
- [46] X. Xia, Y. Lim, P. Zhao, H. Liang, X. Qu, Y. Chen, H. Liu, L. Zhang, S. Zhang, Y. Kim, J. Meng, At. Data Nucl. Data Tables 121-122 (2018) 1. URL: <https://www.sciencedirect.com/science/article/pii/S0092640X17300451>. doi:10.1016/j.adt.2017.09.001.
- [47] I. Angeli, K. Marinova, At. Data Nucl. Data Tables 99 (2013) 69. URL: <https://www.sciencedirect.com/science/article/pii/S0092640X12000265>. doi:10.1016/j.adt.2011.12.006.
- [48] R. Brockmann, R. Machleidt, Phys. Rev. C 42 (1990) 1965. URL: <https://link.aps.org/doi/10.1103/PhysRevC.42.1965>. doi:10.1103/PhysRevC.42.1965.
- [49] A. Akmal, V. R. Pandharipande, D. G. Ravenhall, Phys. Rev. C 58 (1998) 1804. URL: <https://link.aps.org/doi/10.1103/PhysRevC.58.1804>. doi:10.1103/PhysRevC.58.1804.

Table 4
The comparison of charge radii (in fm) of the selected spherical nuclei.

Nuclei	Expt. ^a	PC-L3 ^b	PC-PK1 ^c	PC-PK1 ^{sd}	PC-PK1 ^{ξe}	PC-X ^f	DD-PC1 ^g	DD-PC1 ^{*h}	DD-PCX ⁱ	PC-F1 ^j	PC-F1 ^{*k}	PC-LA ^l	PC-LA ^{*m}
¹⁶ O	2.6991	2.7662	2.7677	2.7677	2.768	2.7698	2.7472	2.7472	2.759	2.7633	2.7633	2.7528	2.7528
⁴⁰ Ca	3.4776	3.4784	3.4815	3.4815	3.481	3.4832	3.4566	3.4565	3.462	3.4777	3.4777	3.4678	3.4679
⁴² Ca	3.5081	3.4779	3.4805	3.4810	3.482	3.4820	3.4626	3.4627	3.469	3.4778	3.4784	3.4729	3.4730
⁴⁴ Ca	3.5179	3.4807	3.4826	3.4833	3.486	3.4838	3.4709	3.4709	3.478	3.4809	3.4819	3.4810	3.4811
⁴⁶ Ca	3.4953	3.4849	3.4865	3.4870	3.490	3.4870	3.4806	3.4803	3.487	3.4860	3.4871	3.4912	3.4912
⁴⁸ Ca	3.4771	3.4907	3.4890	3.4890	3.494	3.4889	3.4895	3.4895	3.494	3.4906	3.4919	3.5023	3.5024
⁵⁰ Ti	3.5704	3.5496	3.5558	3.5543	3.555	3.5519	3.5696	3.5677	3.568	3.5664	3.5650	3.5868	3.5850
⁵⁸ Ni	3.7757	3.7311	3.7372	3.7359	3.737	3.7301	3.7761	3.7748	3.762	3.7645	3.7654	3.8065	3.8059
⁸⁸ Sr	4.2240	4.2198	4.2247	4.2240	4.223	4.2221	4.2231	4.2225	4.226	4.2269	4.2265	4.2379	4.2374
⁹⁰ Zr	4.2694	4.2633	4.2695	4.2683	4.267	4.2662	4.2664	4.2661	4.268	4.2724	4.2723	4.2847	4.2837
⁹² Mo	4.3151	4.3054	4.3125	4.3109	4.310	4.3080	4.3140	4.3128	4.312	4.3192	4.3182	4.3333	4.3319
¹¹² Sn	4.5948	4.5752	4.5801	4.5826	4.582	4.5794	4.5894	4.5898	4.607	4.5870	4.5886	4.6044	4.6070
¹¹⁶ Sn	4.6250	4.6076	4.6121	4.6148	4.614	4.6125	4.6174	4.6171	4.632	4.6168	4.6167	4.6307	4.6324
¹²² Sn	4.6634	4.6502	4.6561	4.6566	4.657	4.6552	4.6579	4.6575	4.659	4.6549	4.6554	4.6728	4.6726
¹²⁴ Sn	4.6735	4.6637	4.6694	4.6698	4.670	4.6686	4.6714	4.6711	4.673	4.6677	4.6683	4.6864	4.6863
¹³⁸ Ba	4.8378	4.8433	4.8508	4.8501	4.848	4.8479	4.8511	4.8504	4.850	4.8494	4.8488	4.8667	4.8661
¹⁴⁰ Ce	4.8771	4.8799	4.8879	4.8869	4.885	4.8845	4.8879	4.8870	4.886	4.8871	4.8861	4.9037	4.9031
¹⁴⁴ Sm	4.9524	4.9475	4.9544	4.9531	4.951	4.9499	4.9521	4.9507	4.952	4.9547	4.9539	4.9676	4.9662
²⁰² Pb	5.4705	5.4840	5.4908	5.4904	5.490	5.4863	5.4869	5.4866	5.485	5.4892	5.4894	5.4996	5.5018
²⁰⁴ Pb	5.4803	5.4936	5.5005	5.5003	5.500	5.4964	5.4962	5.4961	5.494	5.4987	5.4989	5.5112	5.5114
²⁰⁶ Pb	5.4902	5.5028	5.5098	5.5097	5.509	5.5061	5.5049	5.5048	5.503	5.5078	5.5079	5.5200	5.5201
²⁰⁸ Pb	5.5012	5.5108	5.5185	5.5185	5.518	5.5152	5.5129	5.5129	5.511	5.5162	5.5162	5.5279	5.5278
²¹⁴ Pb	5.5577	5.5702	5.5798	5.5774	5.578	5.5730	5.5711	5.5707	5.565	5.5762	5.5742	5.5813	5.5830
rms		0.0223	0.0222	0.0220	0.022	0.0223	0.0197	0.0196	0.0194	0.0197	0.0194	0.0250	0.0250

^a The experimental data is quoted from the compilation by Angeli & Marinova [47].
See the footnote of Table 2 for further description of the theoretical data.